Journal of Neurochemistry

JOURNAL OF NEUROCHEMISTRY | 2016

doi: 10.1111/jnc.13740

ORIGINAL ARTICLE

Chronic pregabalin treatment decreases excitability of dentate gyrus and accelerates maturation of adult-born granule cells

Augusto Abel Lempel,*,[1,3] Lucia Coll,*,[1] Alejandro F. Schinder,† Osvaldo Daniel Uchitel*,[2] and Joaquin Piriz*,‡,[2]

*Instituto de Fisiología Biología Molecular y Neurociencias (IFIBYNE, UBA-CONICET), Buenos Aires, Argentina

†Fundación Instituto Leloir, Instituto de Investigaciones Bioquímicas de Buenos Aires (IIBBA – CONICET), Buenos Aires, Argentina

‡Instituto de Fisiología y Biofísica "Houssay" (IFIBIO "Houssay", UBA-CONICET), Buenos Aires, Argentina

Abstract

Pregabalin (PGB) is extensively prescribed to treat neurological and neuropsychiatrical conditions such as neuropathic pain, anxiety disorders, and epilepsy. Although PGB is known to bind selectively to the α2δ subunit of voltage-gated calcium channels, there is little understanding about how it exerts its therapeutic effects. In this article, we analyzed the effects of an *in vivo* chronic treatment with PGB over the physiology of dentate gyrus granule cells (DGGCs) using *ex vivo* electrophysiological and morphological analysis in adult mice. We found that PGB decreases neuronal excitability of DGGCs. In addition, PGB accelerates maturation of adult-born DGGCs, an effect that would modify dentate gyrus plasticity. Together, these findings suggest that PGB reduces activity in the dentate gyrus and modulates overall network plasticity, which might contribute to its therapeutic effects.

Keywords: dentate gyrus, Gabapentin, neurogenesis, Pregabalin.

J. Neurochem. (2016) 10.1111/jnc.13740

Pregabalin (PGB), together with its close structural relative Gabapentin, constitutes the family of drugs known as gabapentinoids. These drugs are specific ligands of the voltage-dependent calcium channel (VDCC) accessory subunit α2δ(Gee *et al.* 1996; Li *et al.* 2011). PGB is the most prescribed gabapentinoid and constitutes the first choice for the treatment of neuropathic pain, refractory focal seizures and secondary generalized tonic-clonic seizures. In addition, it is used as an alternative or supplementary drug for anxiety disorders (Kawalec *et al.* 2015).

Despite its broad clinical use and its defined molecular targets, the neurophysiological mechanisms of action of PGB remain unknown. Experimental evidences accumulated so far have delineated two potential pathways in which binding of PGB to α2δ could modulate neuronal function. First, PGB has been shown to reduce VDCC currents, either by direct inhibition of VDCC (Stefani *et al.* 1998; Martin *et al.* 2002; Sutton *et al.* 2002; Di Guilmi *et al.* 2011) or by diminishing surface expression of VDCC (Hendrich *et al.* 2008; Bauer *et al.* 2009; Tran-Van-Minh and Dolphin 2010; Weissmann *et al.* 2013).

On the other hand, the interaction between pre-synaptically expressed α2δ and astrocyte-secreted factor thrombospondin

Received April 22, 2016; revised manuscript received June 12, 2016; accepted July 05, 2016.

Address correspondence and reprint requests to Joaquin Piriz, Grupo de Neurociencias de Sistemas, IFIBIO "Houssay" Facultad de Medicina, UBA, Paraguay 2155, 7° piso, Buenos Aires (C1121ABG), Argentina. E-mail: pirizjoaquin@gmail.com

[1]These authors contributed equally to this work.

[2]These authors contributed equally to this work.

[3]Present address: Solomon H. Snyder Department of Neuroscience, Johns Hopkins University School of Medicine, Baltimore, MD, USA.

Abbreviations used: Arc, activity-regulated cytoskeleton-associated protein; AMPA, α-amino-3-hydroxy-5-methylisoxazole-4-propionate; BrdU, bromodeoxyuridine; Cb, CalbindinD-28k; DCX, doublecortin; DGGCs, dentate gyrus granule cells; DIC, differential interference contrast; GFP, green fluorescent protein; ISI, interspike-interval; PFA, paraformaldehyde; PGB, pregabalin; sEPSCs, spontaneous excitatory currents; VDCC, voltage-dependent calcium channel.

has been shown to be a pro-synaptogenic signal which is antagonized by binding of PGB to α2δ. Thus, the second line of evidences point toward an anti-synaptogenic effect of PGB that could block abnormal synaptic rearrangements following pathological situations. In this regard, neuropathic pain has been associated to up-regulation of α2δ (Boroujerdi *et al.* 2011); thrombospondins (Kim *et al.* 2012; Crosby *et al.* 2015; Pan *et al.* 2015), and dorsal horn synaptogenesis (Crosby *et al.* 2015), being all those changes prevented by gabapentinoid administration (Boroujerdi *et al.* 2011; Crosby *et al.* 2015).

One strategy to study potential effects of PGB over circuits and synaptic rearrangements would be to analyze the effect of the drug over circuits that are basally being sculptured in adult brain. The dentate gyrus is one structure that fulfills that criterion since new neurons are constantly incorporated to the network during adulthood (Zhao *et al.* 2008; Toni and Schinder 2015). Thus, this structure provides a good opportunity to study gabapentinoid effects on neuronal development and particularly synaptogenesis in the adult brain. In addition, the dentate gyrus is involved in pathological conditions treated with PGB like epilepsy or anxiety disorders (Snyder *et al.* 2011).

In this article, we aimed to investigate the effect of an *in vivo* chronic treatment with PGB in the physiology of both mature and developing dentate gyrus granule cells (DGGCs) in the adult mouse. Combining retroviral labeling techniques with morphological and electrophysiological analysis, we found that chronic PGB treatment modifies both intrinsic and synaptic properties of DGGCs, with the general impact of reducing neuronal excitability. In addition, PGB accelerates maturation of newborn DGGCs, an effect that would reduce the time window of heightened plasticity that these cells experience during development and its potential recruitment into aberrant circuits formed under pathological conditions.

Methods

Animals

Animals were provided by the 'Central Bivarium of the School Facultad de Ciencias Exactas y Naturales, University of Buenos Aires'. For all procedures, male mice of strain C57B16/J were used. Experimental procedures followed the guidelines of the USA National Institutes of Health Guide for the Care and Use of Laboratory Animals and were approved by the Animal Care and Use Committees of the University of Buenos Aires (CICUAL). Mice were 5–8 weeks of age by the time of retroviral injection. Groups of 5–7 siblings were randomly split into two groups (one control and one to be treated with PGB) of two or more siblings which were housed separately.

Viral vectors

A replication-deficient retroviral vector based on the Moloney murine leukemia virus was used to express GFP under a CAG promoter. This vector has been shown to drive expression specifically in newborn neurons (Laplagne *et al.* 2006).

Retroviral stereotaxic injections

Mice were anesthetized with 100 mg/kg Ketamine and 10 mg/Kg Xylazine and placed in a stereotaxic setup. 1 μL of retroviral vector solution was infused at an approximate speed of 0.15 μL/min into the dorsal area of the dentate gyrus (stereotaxic coordinates: 2 mm posterior to bregma, 1.5 mm lateral to midline, and 1.9 mm below cortical surface) using microcapillar calibrated pipettes.

PGB treatment

PGB treatment started 7–8 days after retroviral injection and continued until mice were killed on recording day (13–15 days). Mice on the PGB-treated group were housed separately from control mice and were offered a solution of 1.33 mg/mL PGB on sterile water as their only source of water. PGB is very stable in aqueous solution (Gujral *et al.* 2009) and is efficiently assimilated when ingested orally (Ben-Menachem 2004) making drinking water an ideal delivery system. Mice ingested an average of 5 mL of water a day (water ingestion did not differ between control and PGB-treated groups) meaning they received an approximate dose of 6.5 mg/day or 325 mg/kg day (assuming an average weight of 20 g).

Whole-cell patch recordings of adult and newborn DGGCs

Mice were anesthetized with 2% Avertin and perfused transcardially with 25 mL of perfusion solution (composition in mM: sucrose 200, KCl 2.5, $NaHCO_3$ 26, NaH_2PO_4 1.25, glucose 20, ascorbic acid 0.4, pyruvic acid 2, $CaCl_2$ 1, $MgSO_4$ 3, and kynurenic acid 1) at 0 to −4°C, pH 7.4 and constantly bubbled with 95% O_2 and 5% CO_2. After perfusion mouse brains were quickly removed and placed on low sodium aCSF (composition in mM: sucrose 250, KCl 2.5, $NaHCO_3$ 26, NaH_2PO_4 1.25, glucose 20, ascorbic acid 0.4, Mio-Inositol 3, pyruvic acid 2, $MgCl_2$ 1, $CaCl_2$ 1) at 4°C, pH 7.4 and constantly bubbled with 95% O_2 and 5% CO_2. Coronal slices 400-μm thick containing the hippocampal region were cut using a vibratome and incubated in aCSF (same composition as previous replacing sucrose with NaCl 125 mM) at 37°C, pH 7.4 and constantly bubbled with 95% O_2 and 5% CO_2 for 30 min. For recordings, slices were placed on aCSF plus 100 μM Picrotoxin at 25°C, pH 7.4 and constantly bubbled with 95% O_2 and 5% CO_2. Somata of DGGCs were visualized using an Upright microscope equipped with DIC (differential interference contrast) filters. GFP expression in newborn transfected DGGCs was visualized with epifluorescence. Recordings were done using microelectrodes (5–8 MΩ) pulled from borosilicate glass and filled with either potassium internal solution (Composition in mM: HEPES 10, Phosphocreatine 10, EGTA 0.2, Mg-ATP 2, Li-GTP 0.5, $MgCl_2$ 1, potassium gluconate 110) or cesium internal solution (same composition as previous replacing potassium gluconate with CsCl 110 mM). Cells with an access resistance above 20 MΩ were discarded. Whole-cell recording was performed using an Axopatch 200B amplifier and a Digidata 1200 digitizer. Data were acquired onto a personal computer using pClamp (Molecular Devices, Palo Alto, CA, USA). Data were acquired at an acquisition rate of 20 KHz and filtered at 5 KHz.

Measurement of intrinsic properties

Cells were patched using potassium internal solution and setup was set to current clamp configuration. Recording protocol consisted of current steps of 1 s duration and variable amplitude (−40–70 pA in 10 pA increments) interspaced by 1 s of no current injection.

Membrane resistance was estimated by computing a linear regression between the membrane voltages at the end of the negative current pulses and the pulses amplitude. To analyze neuronal excitability, we quantified the number of spikes fired during the first 200 ms of positive current steps. To analyze spike waveform, the waveform of the first spike fired by each neuron during the protocol was acquired and the positive and negative peaks (relative to a baseline defined as 2 ms before peak), half-width and rise slope were computed.

Measurement of sEPSCs

For these experiments, either potassium or cesium internal solutions were used. Results did not differ between recordings done using different internal solutions (Data not shown). Setup was set to voltage-clamp configuration and the cells were held at a membrane potential of −70 mV. Spontaneous excitatory currents (sEPSC) frequency was quantified offline using Clampfit 10.2 (Molecular Devices). For analysis of sEPSC waveform properties, the waveform of the first 20 events of every cell was aligned and averaged using Clampfit 10.2 template tool. Amplitude, area under waveform, rise slope (calculated between 10 and 90% of amplitude), decay slope (calculated between 90 and 10% of amplitude), and half width were then computed for each neuron's average waveform.

Measurement of elicited post-synaptic currents

For these experiments, the cesium internal solution was used and the setup was set to voltage clamp configuration. A Platinum-Iridium stimulation electrode was placed at the medial end of the perforant tract. Bipolar stimulation pulses were delivered to stimulate axons in the perforant tract forming synapses with recoded DGGCs. For each experiment stimulation amplitude was slowly increased until a reliable post-synaptic current could be elicited in the recorded neuron. Post-synaptic currents were measured at membrane potentials of −60 mV, 0 mV, and +40 mV. For each membrane potential 15 stimuli were performed resulting in 15 measured post-synaptic currents which were averaged to get a mean elicited current for each condition. The mean elicited current at 0 mV potential was subtracted from the +40 mV and −60 mV mean elicited currents. Then the α-amino-3-hydroxy-5-methylisoxazole-4-propionate (AMPA) receptor mediated post-synaptic current was estimated as the peak current in the −60 mV mean elicited current. The NMDA receptor mediated current was estimated by measuring the mean elicited current after 70 ms of stimulation. The ratio of these two measurements was then calculated to get the AMPA to NMDA current ratio of the cell.

Bromodeoxyuridine treatment

Bromodeoxyuridine (BrdU) (Sigma-Aldrich, Buenos Aires, Argentina) was dissolved in 0.9% NaCl and was delivered intraperitoneally twice a day for 2 days at a dose of 50 μg/g. Three weeks after the last injection, mice were anesthetized (Ketamine/Xylazine) and perfused transcardially with 4% paraformaldehyde. Brains were removed and sectioned (40 μm) in a vibrating microslicer (7000smz; Campden Instruments, Sileby, Loughborough, England). One in six sections throughout the hippocampus was studied by immunohistochemistry and confocal microscopy.

Immunofluorescence

To analyze maturational profile of newborn cells, we performed triple immunostaining against BrdU, the marker of immature neurons, Doublecortin, and the markers of mature cells, NeuN or CalbindinD-28k (Cb). Immunostaining was done on 40 μm free-floating coronal sections throughout the fixed brain. Antibodies were applied in Tris-buffered saline with 3% donkey serum and 0.25% Triton X-100. Double- or triple-labeling immunofluorescence was performed using the following primary antibodies: Anti Activity-regulated cytoskeleton-associated protein (Arc; rabbit polyclonal, 1 : 500; Synaptic Systems, Goettingen, Germany), BrdU (rat monoclonal, 1 : 500; Abcam, Cambridge, England), Cb (mouse polyclonal, 1 : 1000; Chemicon, Temecula, CA, USA), doublecortin (goat polyclonal, 1 : 150; Sigma-Aldrich, Buenos Aires, Argentina), GFP (rabbit polyclonal, 1 : 100; Chemicon) and NeuN (mouse polyclonal, 1 : 500; Millipore Corporation, Bedford, MA, USA). For Cb immunolabeling, preincubation with methanol was included to enhance penetrability. The following corresponding secondary antibodies were used: donkey anti-rat Cy3, donkey anti-mouse Cy5, donkey anti-rabbit Cy5 (1 : 500; Jackson Immuno-Research, West Grove, PA, USA), donkey anti-goat Alexa 488 (1 : 500; Molecular Probes, Eugene, OR, USA), goat anti-rabbit Alexa 488 (1 : 500; Chemicon). For BrdU detection before primary antibody incubation, DNA was denatured with 50% formamide in 2× SSC buffer at 65°C for 2 h, washed in 2× SSC for 15 min, incubated in 2N HCl at 37°C for 30 min, and washed in 0.1 M boric acid, pH 8.5, for 10 min. Following this protocol slices were incubated with primary antibodies for 72 h at 4°C, rinsed three times (15 min each) with Tris-buffered saline and incubated with secondary antibodies for 3 h.

Image analysis

Images were obtained using a confocal microscope (Tokyo, Japan) and the program FluoView (Olympus, Tokyo, Japan). Only GFP+ or BrdU+ cells located in the subgranular zone or granule cells layers were included in the analysis. Images were taken at 'z' intervals of 1 μm using a 40× objective [numerical aperture (NA), 1.3; oil-immersion]. For spine counts, we selected GFP+ dendritic segments located in the middle third of the molecular layer. Images were acquired using a 60× objective (NA, 1.4; oil-immersion, digital zoom of 4) and were taken at z-series at 0.1 μm intervals. In all cases, dendrites with high fluorescence intensity were selected to minimize counting errors because of insufficient signal. For dendritic length measurements images were acquired (40×; NA, 1.3; oil-immersion) from 40-μm-thick sections taking z-series at 1 μm intervals. Three-dimensional reconstruction of dendritic segments was performed with the Zeiss (Oberkochen, Germany) LSM Image Browser Software. Spine density analysis was done by manually counting spines in 150 μm dendritic fragments. Arc expression was assessed from x–y projections from confocal z-series. We calculated the proportion of DGCs expressing Arc as follows: the area of the GCL was measured in anterior hippocampal sections and the number of Arc+ cells was counted to obtain the density of Arc+ cells.

Statistics

For those experiments on which properties across neurons were measured, the *N* is reported in both number of neurons and number of mice from which data was collected using the following format: Number of neurons (Number of mice). For all statistical analysis, data from different neurons were considered independent even when recorded from the same animal. While performing the analysis researcher was blind to which group the neuron analyzed belonged.

Sample size was estimated based on previous data from the Schinder group (Mongiat *et al.* 2009). The relative abundance of GFP- neurons compared to GFP+ neurons introduced some imbalance in the number of animals in each group. When testing for the effects of PGB across GFP- and GFP+ cells on a given property (membrane resistance, sEPSC frequency and other characteristics, action potential waveform properties, AMPA/NMDA ratios) we used two-way ANOVA to test for a significant effect of PGB and whether such effect differ between young and mature DGGCs (significance of PGB-GFP interaction). When a significant PGB effect or significant PGB-GFP interaction effect was found in the ANOVA, we use *post hoc t*-test to analyze significant differences between control and PGB conditions for both GFP- and GFP+ cells. For these comparisons, we made a Bonferroni correction of the p-value given that two hypothesis were tested. When a significant effect was found across the GFP variable we only compared across control GFP- and GFP+ cells and no Bonferroni correction was made. When testing for PGB effects in excitability across different current injection conditions for young and adult DGGCs we used a three-way ANOVA with repeated measures across the injected current variable. This test allowed us to analyze not only the effect of PGB on excitability but also whether the effect was different between young and adult DGGCs (PGB-GFP interaction). In addition, we tested for a significant effect of PGB on the GFP+ and GFP-groups independently using two-way ANOVA with repeated measures across the injected current variable. We also used two-way ANOVA to test for excitability differences between control young and adult DGGCs. When testing for PGB effects on synaptic button density and Arc+ cell density between different experimental groups, we used two tailed *t*-tests. When comparing proportion of BrdU+ cells expressing different neuronal markers across groups, we used the non-parametric Rank-sum test.

Results

To analyze the effect of PGB over adult and newborn DGGCs, we performed electrophysiological recordings of developing and mature DGGCs following chronic PGB treatment. To identify newborn DGGCs we infused in the dentate gyrus retroviral vectors encoding GFP (Laplagne *et al.* 2006). Adult-born DGGCs were studied 21 days after retroviral infection, which represents the age of recorded cells at the time of experiments (3-week-old neurons). Infected cells (GFP+) were located predominantly in the inner third of the granule cell layer (Fig. 1a). GFP+ neurons where more excitable than GFP- DGGCs (Fig. 1b) and showed higher input resistance (Fig. 1c). In addition, GFP+ cells showed lower frequency of spontaneous excitatory synaptic currents (Fig. 1d). All those features are in accordance with previously published data for adult-born

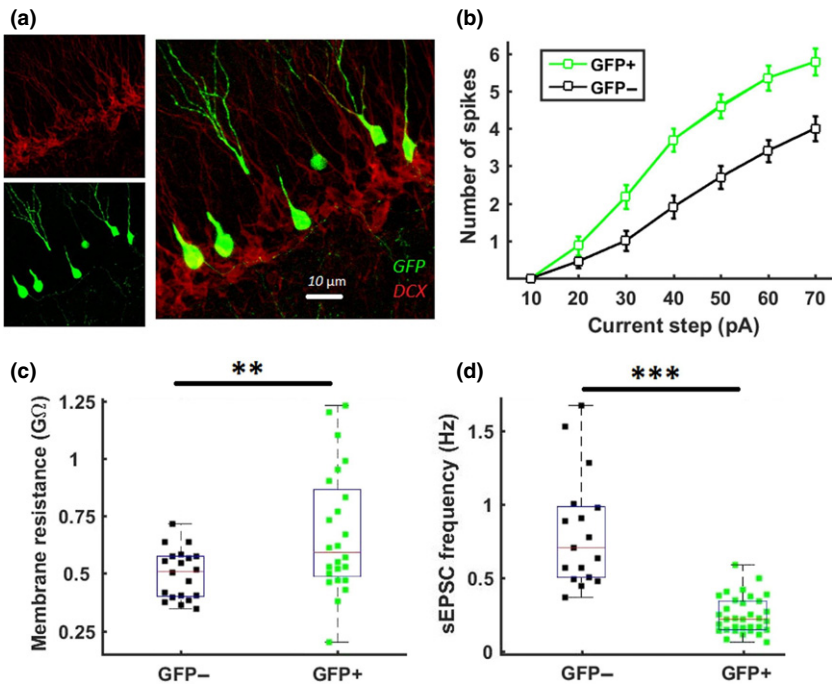

Fig. 1 Characterization of young (GFP+) DGGCs. (a) Double immunostaining against GFP and immature DGGCs marker doublecortin (DCX) of mouse dentate gyrus 21 days after retroviral injection. Transfected newborn DGGCs expressing GFP were located predominantly in the inner zone of the granular layer along with immature DCX+ DGGCs. (b) Mean number of spikes fired during 200 ms depolarizing current pulses of varying amplitude for young (GFP+) and mature (GFP-) DGGCs. Two-way ANOVA with repeated measures GFP-Current interaction $P < 0.001$.N. N: GFP- 20(4), GFP+ 23(14). (c) Boxplots and scatter of individual data points (one per neuron) of membrane resistance. *t*-test $P < 0.01$. N: GFP- 20(4), GFP+ 24(14). (d) Boxplots and scatter of individual data points (one per neuron) of spontaneous excitatory currents (sEPSC) frequency. *t*-test $P < 0.001$. N: GFP- 17(6), GFP+ 33(14).

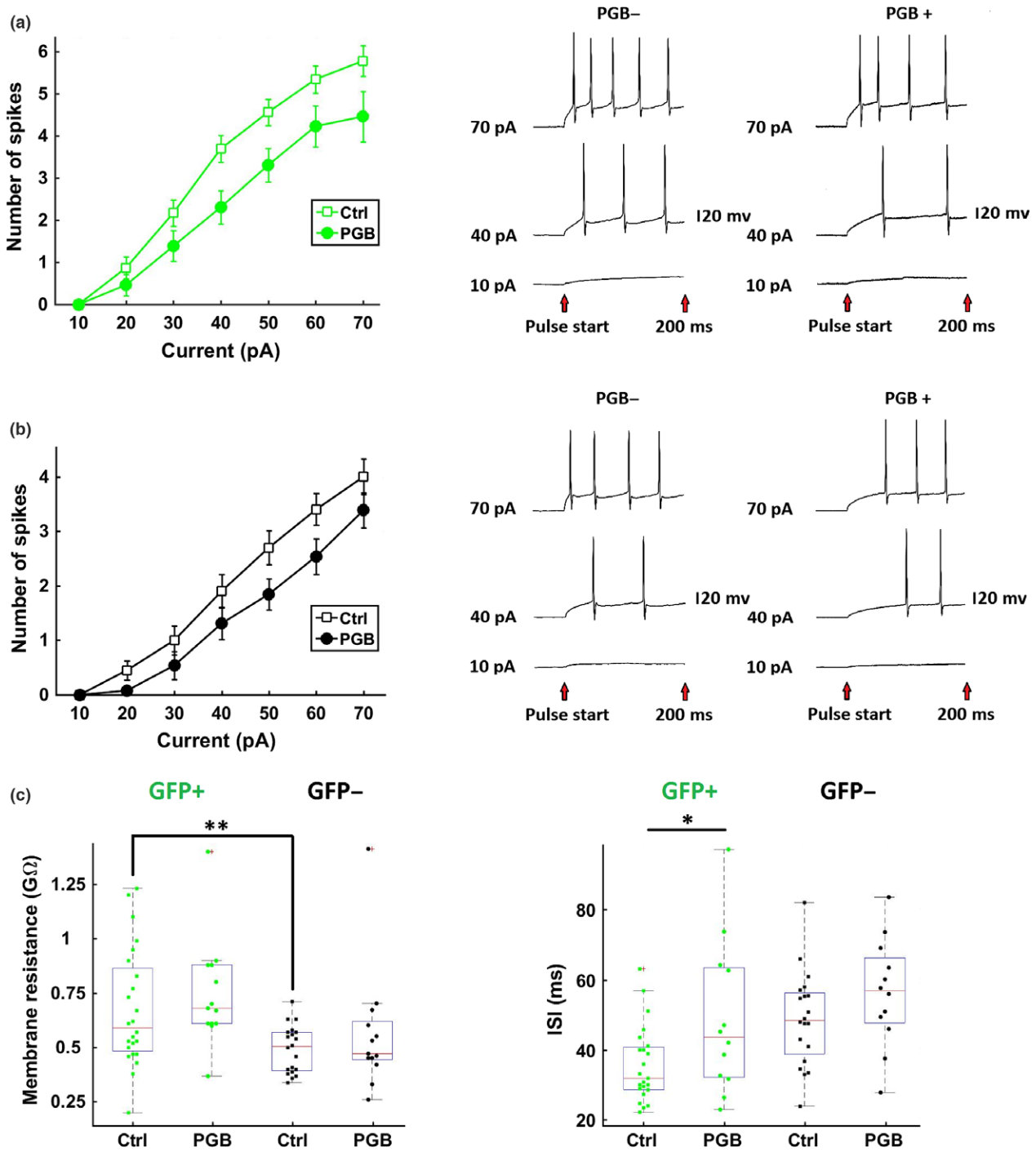

Fig. 2 Characterization of intrinsic excitability in pregabalin (PGB) treated and control DGGCs. (a) Data from developing (GFP+) DGGCs. Left panel, mean number of spikes fired during 200 ms depolarizing current pulses of varying amplitude. Right panel, representative membrane voltage recordings of control and PGB-treated GFP+ DGGCs. Two-way ANOVA with repeated measures for GFP+ neurons: PGB effect $P < 0.05$, PGB-Current interaction $P < 0.01$. N: GFP+ Ctrl 23(14), GFP+ PGB 13(6). (b) Same as A for mature (GFP-) neurons. Two-way ANOVA with repeated measures for GFP- neurons: PGB effect $P = 0.17$, PGB-Current interaction $P = 0.1$. N: GFP- Ctrl 20(4), GFP- PGB 13(6). Three-way ANOVA comparing across GFP+ and GFP-data, PGB effect $P < 0.001$, PGB-Current interaction $P < 0.05$, PGB-GFP interaction $P = 0.1$. (c) Boxplots and scatter of individual data points (one per neuron) for: Left, membrane resistance. Two-way ANOVA PGB effect and PGB-GFP interaction $P > 0.05$. GFP effect $P < 0.05$. *Post hoc t*-test GFP- versus GFP+ $P < 0.01$. N = GFP+ Ctrl 24(14), GFP+ PGB 13(6), GFP- Ctrl 20(4), GFP- PGB 13(6). Right, inter-spike interval (ISI) of spikes fired during 70 pA depolarizing pulses for all experimental groups. *Post hoc t*-test for GFP+ $P < 0.05$. N = GFP+ Ctrl 23(14), GFP+ PGB 12(6), GFP- Ctrl 20(4), GFP- PGB 12(6). $*p < 0.05$ $**p < 0.01$.

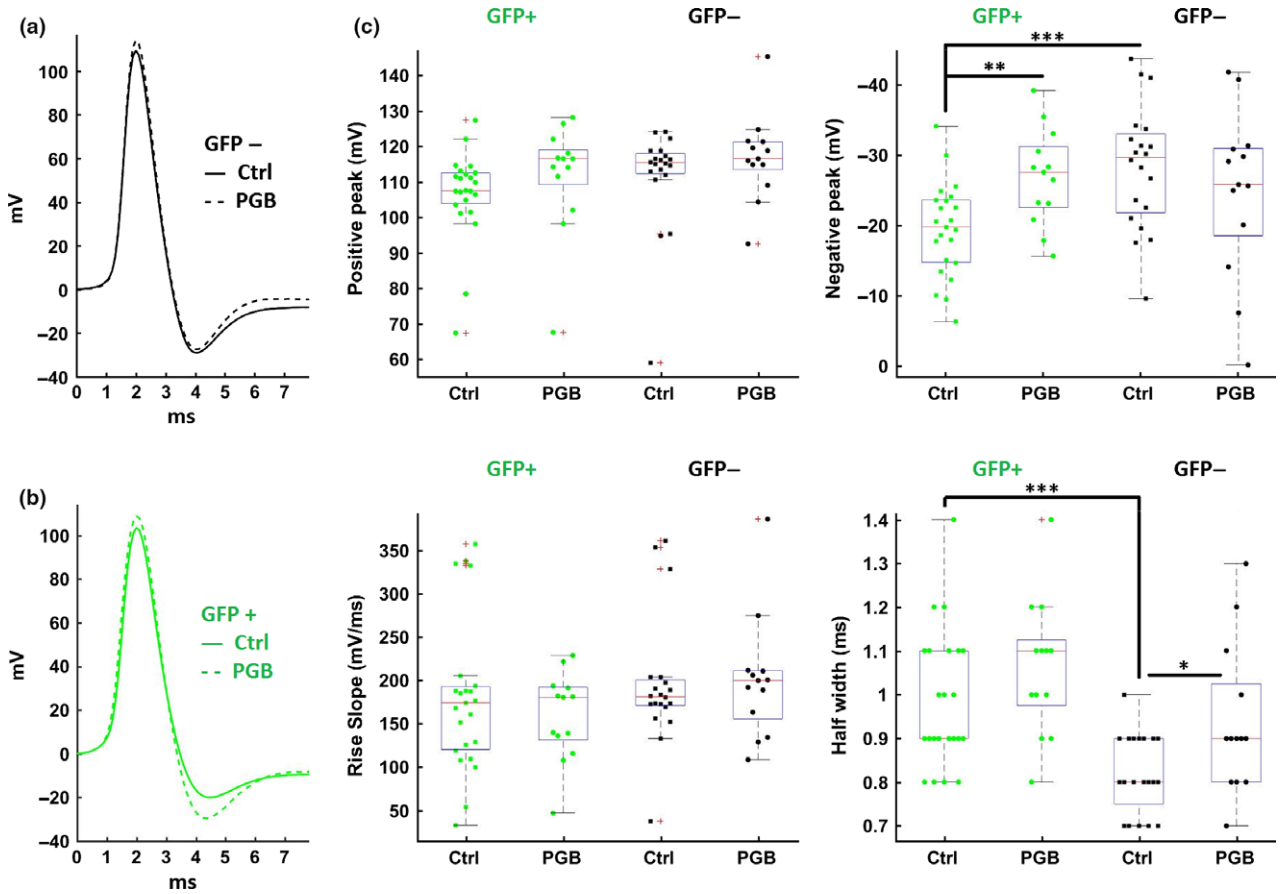

Fig. 3 Characterization of action potential waveform in pregabalin (PGB) treated and control DGGCs. (a) Mean action potential waveform (average across all neurons of each experimental group) of control and PGB-treated mature (GFP-) DGGCs. (b) Same as A for young (GFP+) neurons. (c) Boxplots and scatter of individual data points (one per neuron) of waveform properties. Upper left: positive peak. Two-way ANOVA all P values >0.05. Upper right: Negative peak. Two-way ANOVA PGB-GFP interaction P = 0.01. *Post hoc t*-test GFP- P = 0.4, GFP+ P < 0.01. *Post hoc t*-test Ctrl GFP- versus GFP+ P < 0.001. Lower left: rise slope. Two-way ANOVA all P values >0.05. Lower right: half width. Two-way ANOVA PGB effect P < 0.01, GFP effect P < 0.001, interaction PGB-GFP P = 0.5. *Post hoc t*-test Ctrl versus PGB GFP- P < 0.05; GFP+ P = 0.2. *t*-test Ctrl GFP- versus GFP+ P < 0.001. N: GFP-Ctrl 20(4), GFP- PGB 13(6), GFP+ Ctrl 23(14), GFP+ PGB 13(6). *$p < 0.05$. **$p < 0.01$. ***$p < 0.001$.

immature granule cells, confirming the specificity of the retroviral infection (Espósito *et al.* 2005; Mongiat *et al.* 2009).

One week after virus injection, mice received PGB for 2 weeks through drinking water, while control mice received regular water. Thus, PGB reached developing DGGCs during

Fig. 4 Characterization of synaptic properties in control and pregabalin (PGB) treated young (GFP+) and mature (GFP-) neurons. (a) Representative examples of elicited post-synaptic currents under different membrane voltage (−70 mV α-amino-3-hydroxy-5-methylisoxazole-4-propionate (AMPA), +40 mV NMDA, 0 mV). All traces were normalized to the estimated NMDA current (Marked with a red dot in the graphs, current at +40 mV 70 ms after stimulation). Time 0 is time of fiber stimulation. (b) Boxplots and scatter of individual data points (one per neuron) of AMPA/NMDA current ratio. Two-way ANOVA PGB-GFP interaction P < 0.001. *Post hoc t*-test GFP- P = 0.2, GFP+ P < 0.05. *Post hoc t*-test Ctrl GFP- versus GFP+ P < 0.05. N: GFP-Ctrl 14(4), GFP- PGB 16(14), GFP+ Ctrl 12(6), GFP+ PGB 10(6). (c) Representative examples of voltage clamp recordings used to measure spontaneous excitatory currents (sEPSC) frequency. Single spontaneous excitatory currents were marked in the recordings with a red *. (d) Boxplots and scatter of individual data points (one per neuron) of sEPSC frequency. Two-way ANOVA PGB and GFP effect P < 0.001, PGB-GFP interaction P = 0.7. *Post hoc t*-test GFP- p = 0.06, GFP+ p<0.001. *Post hoc t*-test Ctrl GFP- versus GFP+ P < 0.001. N: GFP- Ctrl 17(5), GFP+ Ctrl 33(14), GFP- PGB 16(6), GFP+ PGB 20(8). (e) Left, Representative examples of dendritic segments of GFP+ neurons in control and PGB-treated mice, synaptic buttons are tagged with green marker. Right, boxplots and scatter of individual data points (one per neuron) for the quantification of synaptic button density in GFP+ neurons of control and PGB-treated mice. *t*-test P = 0.4. N: Ctrl 20(4), PGB 47(4). (f) boxplots and scatter of individual data points (one per neuron) of sEPSC amplitude. Two-way ANOVA all P values >0.05. Same N as D.*$p < 0.05$. **$p < 0.01$ ***$p < 0.001$.

a specific temporal window covering 7–21 days after cell division. During this time DGGCs go through a number of major physiological and anatomical changes including dendritic growth, synaptogenesis, and functional integration (van Praag *et al.* 2002; Espósito *et al.* 2005; Laplagne *et al.* 2006). Twenty-one days after infection we performed electrophysiological recordings of DGGCs in brain slices.

We found that chronic PGB treatment reduced intrinsic excitability of DGCCs. This effect was similar for young and mature DGGCs neurons but reached significance only for

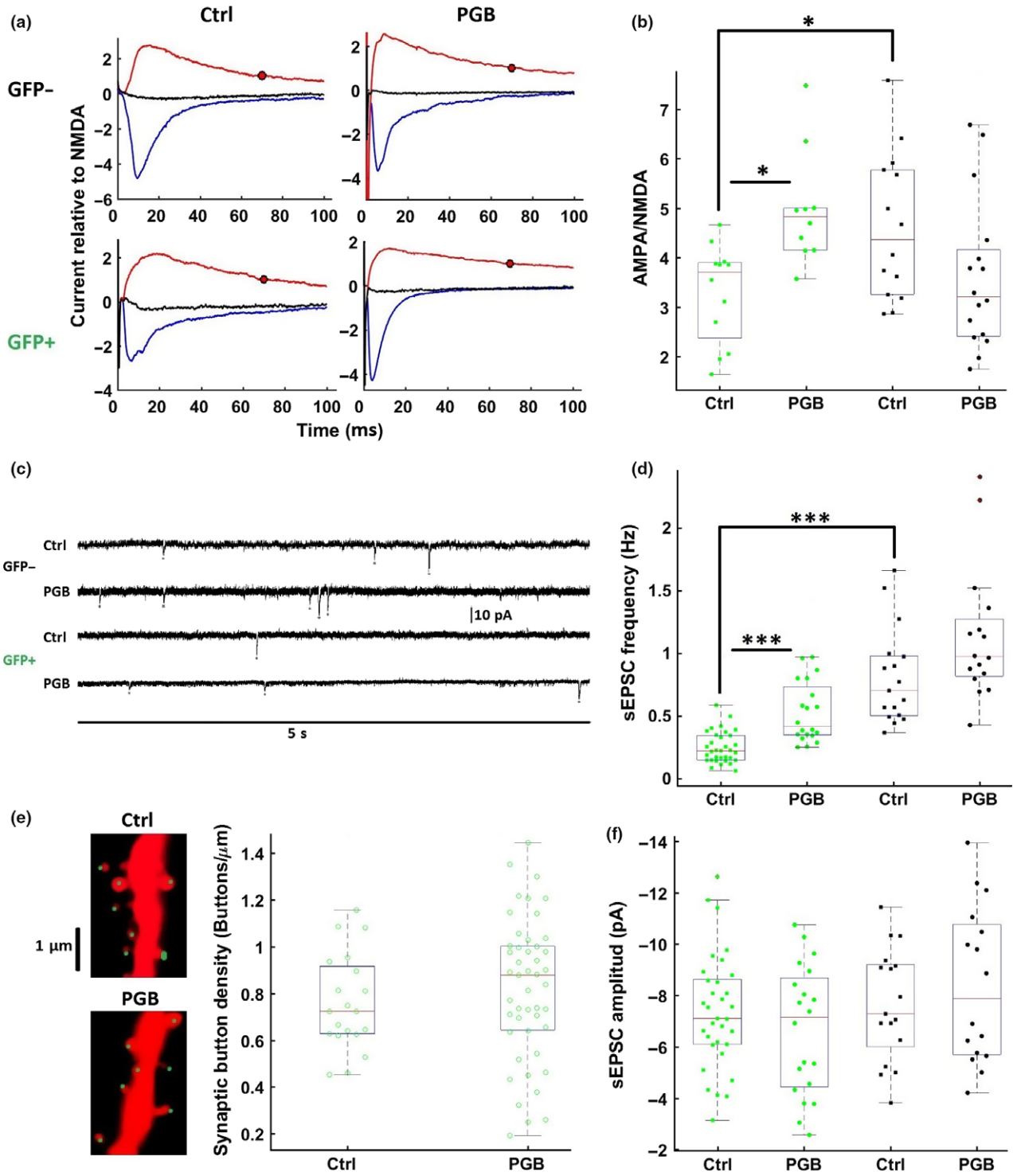

GFP+ neurons (Fig. 2a and b). Reduction in intrinsic excitability in GFP+ neurons was paralleled by an increase in the interspike-interval (analyzed for 70 pA current step) while the input resistance and the minimal current required for action potential firing were not modified (Fig. 2c. Median threshold current for action potential firing was 30 pA for both control and PGB-treated young DGGCs and 40 pA for both control and PGB-treated mature DGGCs, data not shown). Detailed analysis of action potential waveform revealed that PGB treatment slightly increased action potential duration in GFP+ neurons (Fig. 3c). Notably, PGB treatment also increased the hyperpolarization phase action potential in GFP+ neurons (Fig. 3c), a change that could relate to the increase in the inter-spike interval and the decreased excitability.

We further investigated the effects of PGB treatment analyzing excitatory synaptic transmission onto DGGCs. We first measured properties of spontaneous excitatory currents (sEPSCs). PGB increased the frequency of sEPSCs in both mature and developing DGGCs (Fig. 4d). In contrast, other properties of sEPSCs such as amplitude (Fig. 4f) and kinetics (rise slope, decay slope and half width, data not shown) were not modified by PGB. To test whether an increased number of synaptic inputs in young DGGCs could explain the observed increase in sEPSCs frequency, we quantified synaptic button density for GFP+ neurons in control and PGB-treated mice. We found no significant effect of PGB on this morphological property (Fig. 4e). We next analyzed evoked glutamatergic transmission measuring AMPA/NMDA ratio. Notably, PGB treatment affected differentially this parameter in young and mature DGGCs neurons, although when analyzed separately only the effect on young DGGCs reached statistical significance. In young, GFP+ neurons, PGB increased AMPA component of EPSCs while in GFP-neurons there was a tendency to a decrease in AMPA/NMDA ratio (Fig. 4b).

Results presented so far showed two opposing effects of PGB treatment. It decreased intrinsic excitability while increasing spontaneous synaptic transmission. These effects would predict antagonistic changes in network activity. In an attempt to gain insight about the network impact of PGB treatment, we quantified number of DGGCs expressing the marker of neuronal activity Arc (Piatti *et al.* 2011). We found the number of Arc-positive cells in the dentate gyrus to be reduced in PGB-treated animals (Fig. 5b), suggesting that a chronic treatment with PGB would induce an overall reduction in the levels of activity of the dentate gyrus network.

The broad physiological modifications induced by PGB in GFP+ neurons, i.e.: reduced intrinsic excitability, increased hyperpolarization phase of action potential, increased sEPSCs frequency, and increased AMPA/NMDA ratio; are all expected to take place during final maturation of new born DGGCs. To test the idea that PGB treatment speeds up maturation of newly generated DGGCs we labeled them with a single pulse of BrdU and performed PGB treatment as described above. Three weeks after BrdU injection we analyzed expression of molecular markers of neuronal differentiation in DGGCs (von Bohlen Und Halbach 2007). PGB treatment did not modify total number (in cells per 40-μm-thick slice: Control = 80 ± 7, PGB 92 ± 11. *t*-test P = 0.2) or layer distribution of BrdU-positive cells (Fig. 5a). On the other hand, we found PGB treatment increased the number of BrdU cells that express markers of mature DGGCs as NeuN or Calbindin, in expense of a reduction in the number of BrDU-positive cells expressing Doublecortin, a marker of immature DGGCs, (Fig. 5c and d) indicating that treatment with PGB accelerates the rate of maturation of DGGCs.

Discussion

PGB is widely used for the treatment of chronic neurological and neuropsychiatric diseases. Nevertheless, the information available about the neurophysiological consequences of a chronic treatment with PGB is markedly scarce and has been mostly derived from *in vitro* experiments (Hendrich *et al.* 2012; Rossi *et al.* 2013; Valente *et al.* 2012; But see: Zhou and Luo 2015). Our work directly assessed that subject since we described the effect of a chronic PGB treatment over neurophysiological properties of the principal cells of the dentate gyrus, a structure involved in pathological conditions treated with PGB as epilepsy and anxiety disorders (Snyder *et al.* 2011). We found PGB generally decreased intrinsic excitability of DGGCs and increments frequency of sEPSCs. The balance between these two modifications, that would have opposite effects over network activity, bends over an inhibitory effect, as suggested by the reduction in the number of Arc+ cells. In addition, in newborn DGGCs, PGB treatment increased the expression of mature neuronal markers, the after hyperpolarization phase of action potentials, and the AMPA/NMDA ratio. Since all those changes take place during maturation of adult-born DGGCs, we conclude that chronic PGB treatment accelerates maturation of adult-born DGGCs. In this regard, our results agree and extend over previous work showing increased differentiation of neural progenitors into neurons by PGB (Valente *et al.* 2012). Notably, acceleration of DGGCs maturation is paralleled by reduced network activity, a scenario that contradicts what has been observed in physiological conditions, where a positive correlation between network activity and rate of maturation of newborn DGGCs has been described (Piatti *et al.* 2011). It is, therefore, tempting to speculate that a direct action of PGB over newborn DGGCs accelerates their development, which would otherwise be slowed-down by the PGB-induced decrease in dentate network activity. These findings suggest a novel hypothesis about the effects

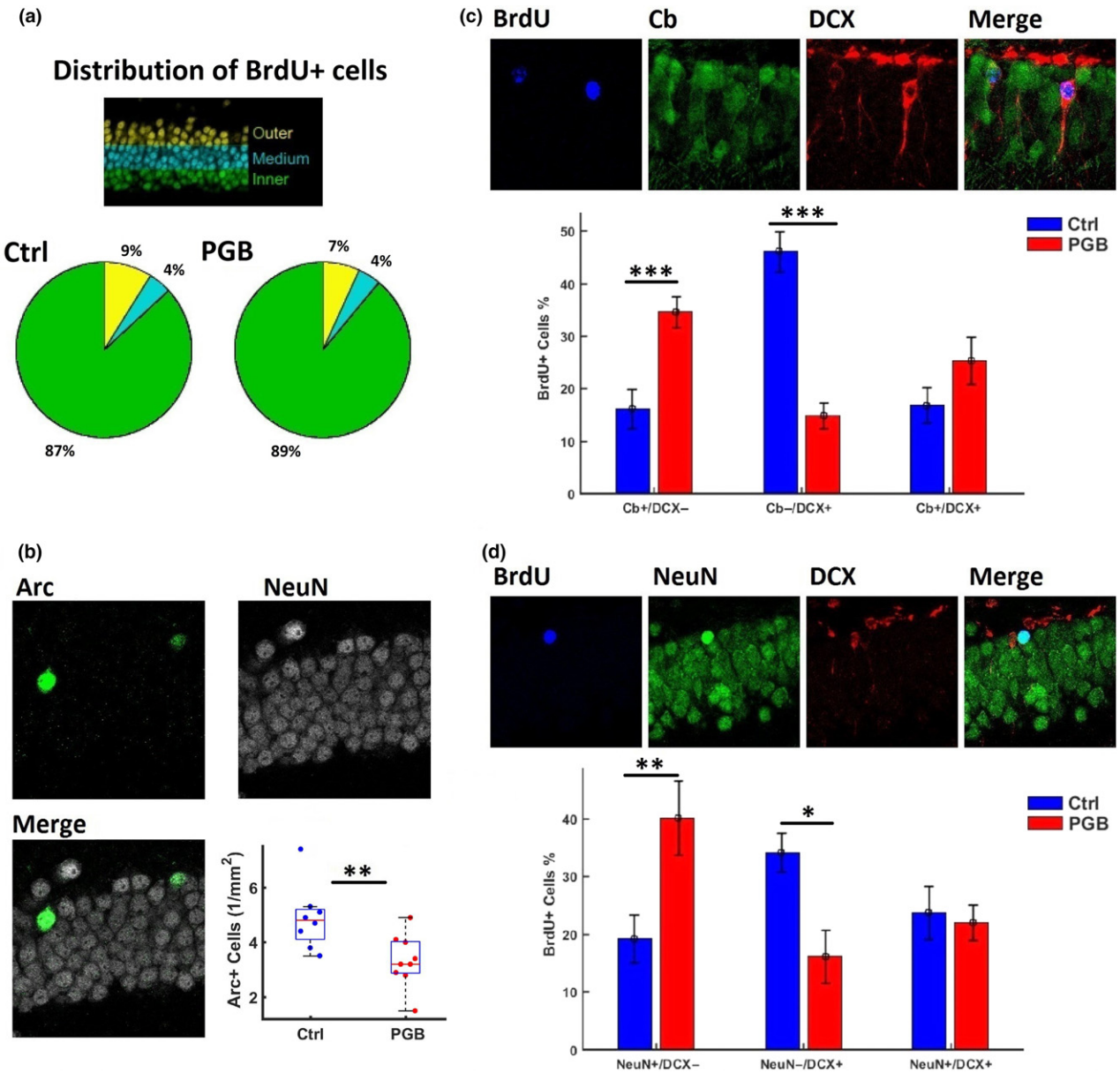

Fig. 5 (a) dentate gyrus layer positioning of bromodeoxyuridine (BrdU)+ neurons in control and pregabalin (PGB) treated mice. (b) Double immunostaining against activity-regulated Arc and neuronal marker NeuN. Lower right panel: density of Arc expressing neurons in dentate gyrus of control and PGB-treated mice. *t*-test $P < 0.01$. N: Control = 8, PGB = 9. (c) Upper panel, double immunostaining against mature granule cells marker Cb and immature granule cells marker doublecortin (DCX) of BrdU-labeled cells. Lower panel, percentage of BrdU-positive granule cells expressing different marker combinations. Increased proportion of Cb+/DCX- in PGB-treated mice Rank-sum test $P < 0.001$. Decreased proportion of Cb-/DCX+ in PGB-treated mice Rank-sum test $P < 0.001$. N: Control = 8, PGB = 9. (d) Upper panel, double immunostaining against mature granule cells marker NeuN and immature granule cells marker DCX of BrdU labeled cells. Lower panel, percentage of BrdU-positive granule cells expressing different marker combinations. Increased proportion of NeuN+/DCX- in PGB-treated mice Rank-sum test $P < 0.01$. Decreased proportion of NeuN-/DCX+ in PGB-treated mice Rank-sum test $P = 0.01$. N: Control = 7, PGB = 7. $*p < 0.05$. $**p < 0.01$ $***p < 0.001$.

of PGB on the dentate gyrus: developing DGGCs go through a period of high activity and synaptic plasticity that favors their recruitment that makes them a critical component of dentate gyrus network (Mongiat *et al.* 2009; Marín-Burgin *et al.* 2012). Accelerating their maturation by PGB would effectively shorten their window of sensitivity of those young-highly recruitable neurons, thus reducing the plasticity and overall activity of the dentate gyrus. In a

pathological context, such as epilepsy, this decrease in synaptic plasticity may have therapeutic effects. In this regard, recent reports have demonstrated that aberrant neurogenesis may contribute to the generation of spontaneous recurrent seizures (Cho *et al.* 2015), indicating that a reduction in the number of immature DGGCs could have an antiepileptic effect. Then it is plausible that reducing the period of heightened plasticity of newborn DGCCs could have a similar impact. To test that hypothesis it would be necessary to assess the effect of PGB on chronic proliferation and organization of new neurons generated after epileptic episodes.

It has been firmly established that PGB and Gabapentin, its close relative, exert their effects through α2δ (Stahl *et al.* 2013). However, the cellular mechanisms of action of these drugs have not been elucidated, a situation directly derived from to the little understanding about the cellular function of α2δ. This protein has been identified both as a regulatory subunit of VDCC and as a pro synaptogenic factor (Stahl *et al.* 2013). Notably the latter function of α2δ is totally independent of VDCC (Eroglu *et al.* 2009). Moreover, PGB has been shown to both reduce VDCC currents (Stefani *et al.* 1998; Martin *et al.* 2002; Sutton *et al.* 2002; Di Guilmi *et al.* 2011) and to inhibit α2δ thromobospondin mediated synaptogenesis (Eroglu *et al.* 2009; Crosby *et al.* 2015). The relative contribution of these two potential mechanisms of action of PGB to its therapeutic effects has not been studied. Our study provides some information about that subject. In the dentate gyrus, plastic changes and synaptogenesis during adulthood could be readily predicted offering the possibility to compare the effects of long-term PGB treatment with well described control conditions (Espósito *et al.* 2005). Our results suggest that PGB treatment induces general plastic changes over DGGCs. The effects of PGB that we describe could not be directly explained by a reduction in VDCCs currents since we found modification in both intrinsic and synaptic features with even opposite signs in young and adult DGCCs. Using the same argument our results could not be explained solely based on the modulation of synaptogenesis, particularly since we found no changes in spine density in new born DGGCs. Therefore, our work strongly suggests that chronic PGB treatment exerts complex effects that could not be directly predicted by either antagonisms of VDCC or synaptogenesis. A deeper analysis of the mechanisms of action of PGB could derive into rationally improved designs of new gabapentinoids.

In conclusion, in this work we characterize for the first time from the neurophysiological point of view the consequences of a chronic treatment with PGB on DGGCs. We found PGB decreases excitability and accelerates maturation of adult-born neurons. This action of PGB would have a long-term effect over dentate gyrus network, which might be related to its action as an antiepileptic and anxiolytic drug.

Acknowledgments and conflict of interest disclosure

We thank Mariela F. Trinchero and Antonia Marin-Burgin for insightful experimental advice and suggestions, and Natalia Beltramone for making retroviral preparations. This work was supported by National Agency for Promotion of Science and Technology (ANPCyT) grants BID PICT 2013-2202 (to ODU), BID PICT 2011-2667 (to ODU), BID PICT 2012-1931 (to JP); University of Buenos Aires grant UBACyT 20020130100666BA (to ODU) and CONICET grant PIP-11220110100768 (to ODU and JP). The authors have no conflict of interest to declare.

All experiments were conducted in compliance with the ARRIVE guidelines.

References

Bauer C. S., Nieto-Rostro M., Rahman W., Tran-Van-Minh A., Ferron L., Douglas L., Kadurin I. *et al.* (2009) The increased trafficking of the calcium channel subunit alpha2delta-1 to presynaptic terminals in neuropathic pain is inhibited by the alpha2delta ligand pregabalin. *J. Neurosci.* **29**, 4076–4088.

Ben-Menachem E. (2004) Pregabalin pharmacology and its relevance to clinical practice. *Epilepsia* **45**(Suppl 6), 13–18.

von Bohlen Und Halbach O. (2007) Immunohistological markers for staging neurogenesis in adult hippocampus. *Cell Tissue Res.* **329**, 409–420.

Boroujerdi A., Zeng J., Sharp K., Kim D., Steward O. and Luo Z. D. (2011) Calcium channel alpha-2-delta-1 protein upregulation in dorsal spinal cord mediates spinal cord injury-induced neuropathic pain states. *Pain* **152**, 649–655.

Cho K.-O., Lybrand Z. R., Ito N., Brulet R., Tafacory F., Zhang L., Good L. *et al.* (2015) Aberrant hippocampal neurogenesis contributes to epilepsy and associated cognitive decline. *Nat. Commun.* **6**, 6606.

Crosby N. D., Zaucke F., Kras J. V., Dong L., Luo Z. D. and Winkelstein B. A. (2015) Thrombospondin-4 and excitatory synaptogenesis promote spinal sensitization after painful mechanical joint injury. *Exp. Neurol.* **264**, 111–120.

Di Guilmi M. N., Urbano F. J., Inchauspe C. G. and Uchitel O. D. (2011) Pregabalin modulation of neurotransmitter release is mediated by change in intrinsic activation/inactivation properties of Cav2.1 calcium channels. *J. Pharmacol. Exp. Ther.* **336**, 973–982.

Eroglu Ç., Allen N. J., Susman M. W., O'Rourke N. A., Park C. Y., Özkan E., Chakraborty C. *et al.* (2009) The gabapentin receptor α2δ-1 is the neuronal thrombospondin receptor responsible for excitatory CNS synaptogenesis. *Cell* **139**, 380–392.

Espósito M. S., Piatti V. C., Laplagne D. A., Morgenstern N. A., Ferrari C. C., Pitossi F. J. and Schinder A. F. (2005) Neuronal differentiation in the adult hippocampus recapitulates embryonic development. *J. Neurosci.* **25**, 10074–10086.

Gee N. S., Brown J. P., Dissanayake V. U., Offord J., Thurlow R. and Woodruff G. N. (1996) The novel anticonvulsant drug, gabapentin (Neurontin), binds to the alpha2delta subunit of a calcium channel. *J. Biol. Chem.* **271**, 5768–5776.

Gujral R. S., Haque S. M. and Shanker P. (2009) Development and validation of pregabalin in bulk, pharmaceutical formulations and in human urine samples by UV spectrophotometry. *Int. J. Biomed. Sci.* **5**, 175–180.

Hendrich J., Van Minh A. T., Heblich F., Nieto-Rostro M., Watschinger K., Striessnig J., Wratten J., Davies A. and Dolphin A. C. (2008) Pharmacological disruption of calcium channel trafficking by the α2δ ligand gabapentin. *Proc. Natl Acad. Sci.* **105**, 3628–3633.

Hendrich J., Bauer C. S. and Dolphin A. C. (2012) Chronic pregabalin inhibits synaptic transmission between rat dorsal root ganglion and dorsal horn neurons in culture. *Channels (Austin)* **6**, 124–132.

Kawalec P., Cierniak A., Pilc A. and Nowak G. (2015) Pregabalin for the treatment of social anxiety disorder. *Expert Opin. Investig. Drugs* **24**, 585–594.

Kim D.-S., Li K.-W., Boroujerdi A., Yu Y. P., Zhou C.-Y., Deng P., Park J. *et al.* (2012) Thrombospondin-4 contributes to spinal sensitization and neuropathic pain states. *J. Neurosci.* **32**, 8977–8987.

Laplagne D. A., Espósito M. S., Piatti V. C., Morgenstern N. A., Zhao C., Praag H. van., Gage F. H. and Schinder A. F. (2006) Functional convergence of neurons generated in the developing and adult hippocampus. *PLoS Biol.* **4**, e409.

Li Z., Taylor C. P., Weber M., Piechan J., Prior F., Bian F., Cui M., Hoffman D. and Donevan S. (2011) Pregabalin is a potent and selective ligand for α(2)δ-1 and α(2)δ-2 calcium channel subunits. *Eur. J. Pharmacol.* **667**, 80–90.

Marín-Burgin A., Mongiat L. A., Pardi M. B. and Schinder A. F. (2012) Unique processing during a period of high excitation/inhibition balance in adult-born neurons. *Science* **335**, 1238–1242.

Martin D. J., McClelland D., Herd M. B., Sutton K. G., Hall M. D., Lee K., Pinnock R. D. and Scott R. H. (2002) Gabapentin-mediated inhibition of voltage-activated Ca2 + channel currents in cultured sensory neurones is dependent on culture conditions and channel subunit expression. *Neuropharmacology* **42**, 353–366.

Mongiat L. A., Espósito M. S., Lombardi G. and Schinder A. F. (2009) Reliable activation of immature neurons in the adult hippocampus. *PLoS ONE* **4**, e5320.

Pan B., Yu H., Park J., Yu Y. P., Luo Z. D. and Hogan Q. H. (2015) Painful nerve injury upregulates thrombospondin-4 expression in dorsal root ganglia. *J. Neurosci. Res.* **93**, 443–453.

Piatti V. C., Davies-Sala M. G., Espósito M. S., Mongiat L. A., Trinchero M. F. and Schinder A. F. (2011) The timing for neuronal maturation in the adult hippocampus is modulated by local network activity. *J. Neurosci.* **31**, 7715–7728.

van Praag H., Schinder A. F., Christie B. R., Toni N., Palmer T. D. and Gage F. H. (2002) Functional neurogenesis in the adult hippocampus. *Nature* **415**, 1030–1034.

Rossi A. R., Angelo M. F., Villarreal A., Lukin J. and Ramos A. J. (2013) Gabapentin administration reduces reactive gliosis and neurodegeneration after pilocarpine-induced status epilepticus. *PLoS ONE* **8**, e78516.

Snyder J. S., Soumier A., Brewer M., Pickel J. and Cameron H. A. (2011) Adult hippocampal neurogenesis buffers stress responses and depressive behaviour. *Nature* **476**, 458–461.

Stahl S. M., Porreca F., Taylor C. P., Cheung R., Thorpe A. J. and Clair A. (2013) The diverse therapeutic actions of pregabalin: is a single mechanism responsible for several pharmacological activities?. *Trends Pharmacol. Sci.* **34**, 332–339.

Stefani A., Spadoni F. and Bernardi G. (1998) Gabapentin inhibits calcium currents in isolated rat brain neurons. *Neuropharmacology* **37**, 83–91.

Sutton K. G., Martin D. J., Pinnock R. D., Lee K. and Scott R. H. (2002) Gabapentin inhibits high-threshold calcium channel currents in cultured rat dorsal root ganglion neurones. *Br. J. Pharmacol.* **135**, 257–265.

Toni N. and Schinder A. F. (2015) Maturation and functional integration of new granule cells into the adult hippocampus. *Cold Spring Harb. Perspect. Biol.* **8**, a018903.

Tran-Van-Minh A. and Dolphin A. C. (2010) The alpha2delta ligand gabapentin inhibits the Rab11-dependent recycling of the calcium channel subunit alpha2delta-2. *J. Neurosci.* **30**, 12856–12867.

Valente M. M., Bortolotto V., Cuccurazzu B., Ubezio F., Meneghini V., Francese M. T., Canonico P. L. and Grilli M. (2012) α2δ ligands act as positive modulators of adult hippocampal neurogenesis and prevent depression-like behavior induced by chronic restraint stress. *Mol. Pharmacol.* **82**, 271–280.

Weissmann C., Di Guilmi M. N., Urbano F. J. and Uchitel O. D. (2013) Acute effects of pregabalin on the function and cellular distribution of Ca(V)2.1 in HEK293t cells. *Brain Res. Bull.* **90**, 107–113.

Zhao C., Deng W. and Gage F. H. (2008) Mechanisms and functional implications of adult neurogenesis. *Cell* **132**, 645–660.

Zhou C. and Luo Z. D. (2015) Nerve injury-induced calcium channel alpha-2-delta-1 protein dysregulation leads to increased pre-synaptic excitatory input into deep dorsal horn neurons and neuropathic allodynia. *Eur. J. Pain* **19**, 1267–1276.

